Supporting Information

Visible Light-induced Water Oxidation Catalyzed by Molybdenum-based Polyoxometalates with Mono- and Dicobalt(III) Cores as Oxygen-Evolving Centers

Saya Tanaka[a], Masahiko Annaka[ab] and Ken Sakai*[ab]

[a] Department of Chemistry, Faculty of Science, Kyushu University,
6-10-1 Hakozaki, Higashi-ku, Fukuoka, 812-8581, Japan
[b] International Research Center for Molecular Systems (IRCMS), Kyushu University,
Motooka 744, Nishi-ku, Fukuoka, 819-0395, Japan

E-mail: ksakai@chem.kyushu-univ.jp

Experimental

Materials

All solvents and reagents were of the highest quality available and were used as received. $H_3[PMo_{12}O_{40}]$ and $(NH_4)_6[Mo_7O_{24}] \cdot 4H_2O$ were purchased from Kanto Chemical Co., Inc. and were used as received. $[Ru(bpy)_3](NO_3)_2 \cdot 3H_2O$ was prepared as previously described.[1]

Measurements

UV-Visible absorption spectra were recorded on a Shimadzu UV2450SIM spectrophotometer. All the sample solutions were thermostated at 20 °C during the spectrometric measurements. The electrochemical studies were carried out for the argon-purged aqueous solution of catalysts (1 mM). Dynamic light scattering (DLS) experiments were carried out using a DLS/SLS-5000 (ALV, Langen, Germany) photometer. A 22 mW He-Ne laser (Uniphase, U.S.A.) operating at 632.8 nm was used. In the DLS experiments, the full homodyne intensity autocorrelation function was determined with an ALV-5000 multiple-τ-digital correlator. Data were obtained using a scattering angle 90° at 23 °C. The DLS measurements were carried out for the aqueous borate buffer solution (pH = 8.0) of **Co$_n$-POM-Mo**'s containing $[Ru(bpy)_3](NO_3)_2 \cdot 3H_2O$ (0.06 mM). The solids deposited upon mixing **Co$_n$-POM-Mo**'s and $Ce(NH_4)_2(NO_3)_6$ were analyzed by using energy dispersive X-ray fluorescence spectroscopy (a Shimadzu EDX-720 spectrometer). The measurement was carried out in air. The quantitative analysis of the elements involved in the bulk samples was carried out by use of the fundamental parameter (FP) method implemented in this setup, without preparing any standard materials. The FP method is considered as a powerful method in giving somewhat reliable results.

Photolysis Experiments

Photochemical oxygen production from water was analyzed by using an automatic O_2 monitoring system developed in our group. In this system, continuous flow of Ar (10.0 mL/min, controlled by a STEC SEC-E40/PAC-D2 digital mass flow controller) was bubbled through a photolysis solution (10 mL) contained in a Pyrex vial (*ca.* 20 mL). The vent gas from the vial was introduced into a valve which allowed the automatic injection of the sample gas onto a gas chromatograph (Shimadzu GC-8A equipped with a molecular sieve 5A column of 2 m × 3 mm *i.d.*, thermostated at 30 ºC). The injection of the sample gas was controlled by a control software operating on a Windows system and the output signal from the thermal conductivity detector of the gas chromatograph was analyzed in a Shimadzu chromatopac C-R8A which was also controlled within the same control program. Photolysis solutions were deaerated with Ar for at least 30 min prior to the photolysis. The photoirradiation was carried out by an ILC Technology CERMAX LX-300 300 W Xe lamp equipped with a CM-1 cold mirror (400 < λ < 800 nm). The photolysis vial was immersed in a water bath thermostated at 20 ºC to remove IR radiation and to eliminate the temperature effect. The quantum yields for the photochemical O_2 evolution ($\Phi(O_2)$) were determined by the photoirradiation of the MLCT band of $Ru(bpy)_3^{2+}$, where the light source (400 < λ < 490 nm) was provided by combining an interference filter (Asahi Spectra SV 490) with the Xe source described above. The photon flux from this light source was determined using the ferrioxalate chemical actinometry.[2]
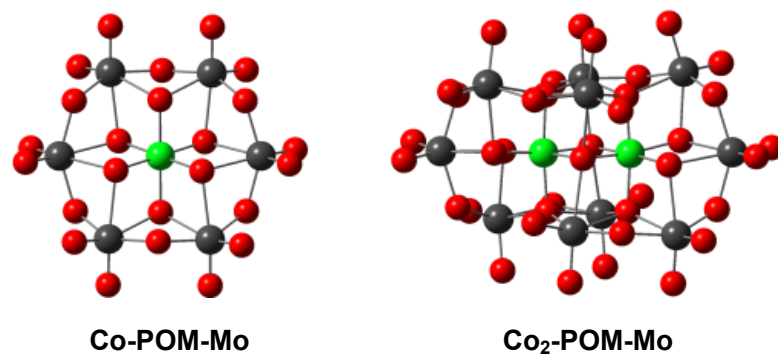
Co-POM-Mo   **Co₂-POM-Mo**

Scheme S1. The structures of Anderson- (**Co-POM-Mo**) and Evans-Showell-type (**Co₂-POM-Mo**) polyoxometalates (Co: green; Mo: gray; O: red). The structures are shown omitting hydrogen atoms, water molecules, and ammonium cations.
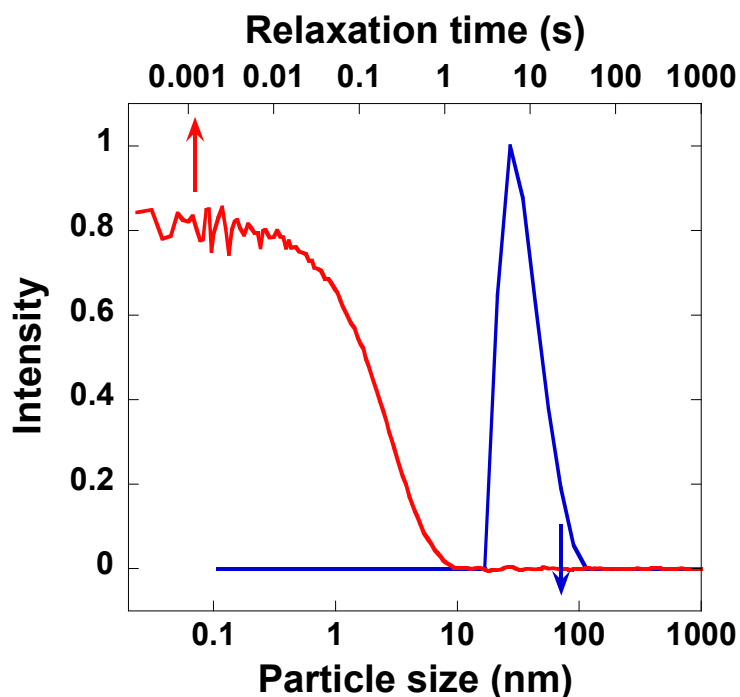
Fig. S1 Autocorrelation function (red line) obtained by the dynamic light scattering (DLS) for an aqueous borate buffer solution (0.1 M, pH = 8.0) containing $[Co(OH_2)_6](NO_3)_2$ (10 μM) after 30-sec irradiation with 300 W Xe lamp and relaxation spectrum (blue line) calculated from the autocorrelation function. The data confirm that the formation of CoO_x from $[Co(OH_2)_6](NO_3)_2$ is effectively promoted upon the photoirradiation. The same experiments were also conducted by use of **Co-POM-Mo** and **Co$_2$-POM-Mo** by adopting the experimental conditions used in the O_2 evolution experiments in this study, in which we confirmed that the corresponding relaxation spectra could not be obtained due to the too low scattering intensities for these cases. With these results, we can judge that CoO_x nanoparticles are not given when **Co-POM-Mo** and **Co$_2$-POM-Mo** are employed as molecular catalysts for O_2 evolution.
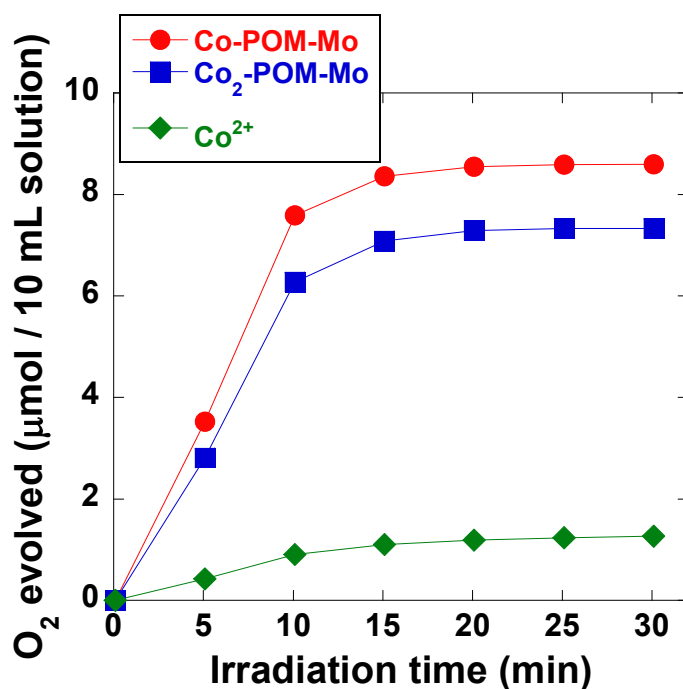
Fig. S2 Photochemical O_2 production from an aqueous borate buffer solution (0.1 M, pH = 8.0; 10 mL) containing $Na_2S_2O_8$ (3.0 mM) and $[Ru(bpy)_3](NO_3)_2 \cdot 3H_2O$ (0.06 mM) in the presence of $[Co(OH_2)_6](NO_3)_2$ (20 μM; ♦), which presumably affords CoO_x as an active species during the photolysis, even though the activity is much lower than those observed for the systems catalyzed by **Co_n-POM-Mo**'s; **Co-POM-Mo** (20 μM; ●) and **Co_2-POM-Mo** (10 μM; ■) in Ar at 20 ℃ (irradiation with 300 W Xe lamp; 400−800 nm). The data for the latter two are same to those depicted in Figs. S8 and S9. The above DLS data clearly reveal that the formation of CoO_x is obvious for the $[Co(OH_2)_6]^{2+}$ system. The lower O_2-evolving activity observed here rather demonstrates that the CoO_x species photochemically generated under these photolysis conditions possess quite low activity as catalysts for O_2 evolution. These further strengthen the idea that the **Co_n-POM-Mo**'s rather than CoO_x are serving as active catalysts for O_2 evolution under these conditions.
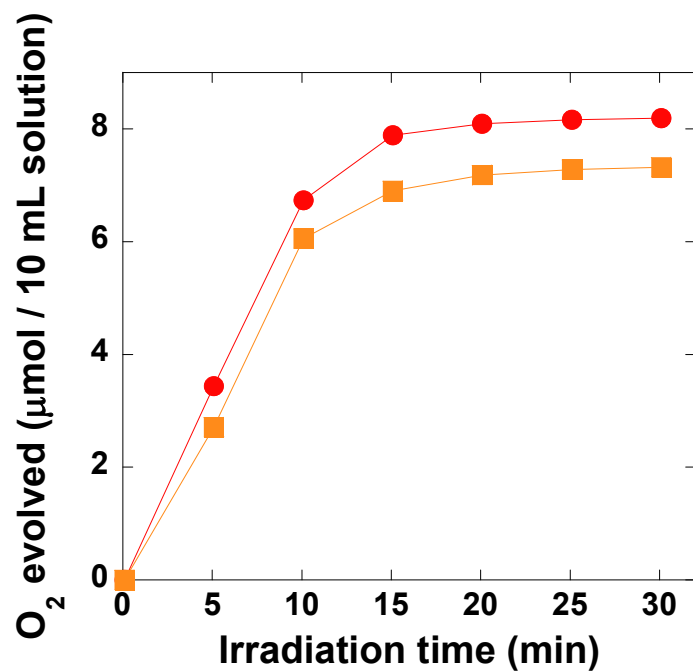
Fig. S3 Photochemical O_2 production for the first run (●) and second run (■) from an aqueous borate buffer solution (0.1 M, pH = 8.0; 10 mL) containing [Ru(bpy)$_3$](NO$_3$)$_2$·3H$_2$O (0.3 mM), Na$_2$S$_2$O$_8$ (3.0 mM) and **Co-POM-Mo** (20 μM) in Ar at 20 °C (irradiation with 300 W Xe). After the completion of the first run, 3 mM of Na$_2$S$_2$O$_8$ was added to the reaction solution.
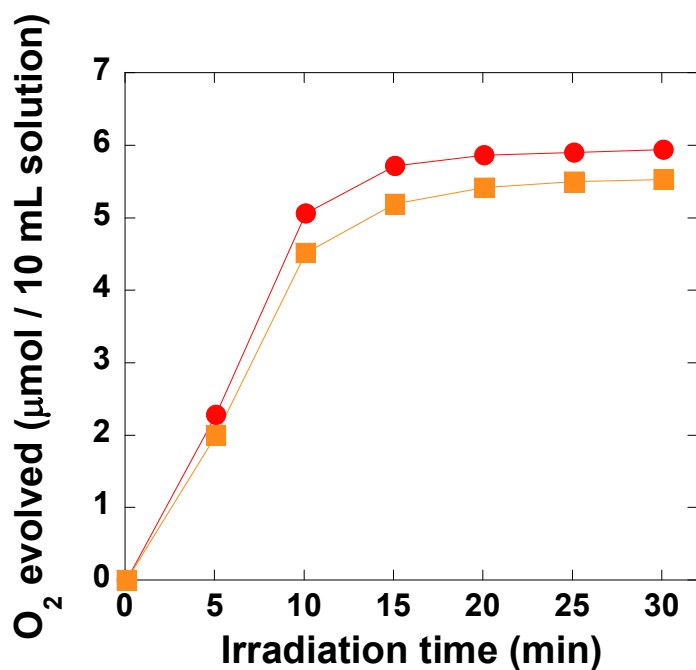
Fig. S4 Photochemical O_2 production of the first run (●) and second run (■) from an aqueous borate buffer solution (0.1 M, pH = 8.0; 10 mL) containing $[Ru(bpy)_3](NO_3)_2 \cdot 3H_2O$ (0.3 mM), $Na_2S_2O_8$ (3.0 mM) and **Co$_2$-POM-Mo** (20 μM) in Ar at 20 °C (irradiation with 300 W Xe). After the completion of the first run, 3 mM of $Na_2S_2O_8$ was added to the reaction solution.
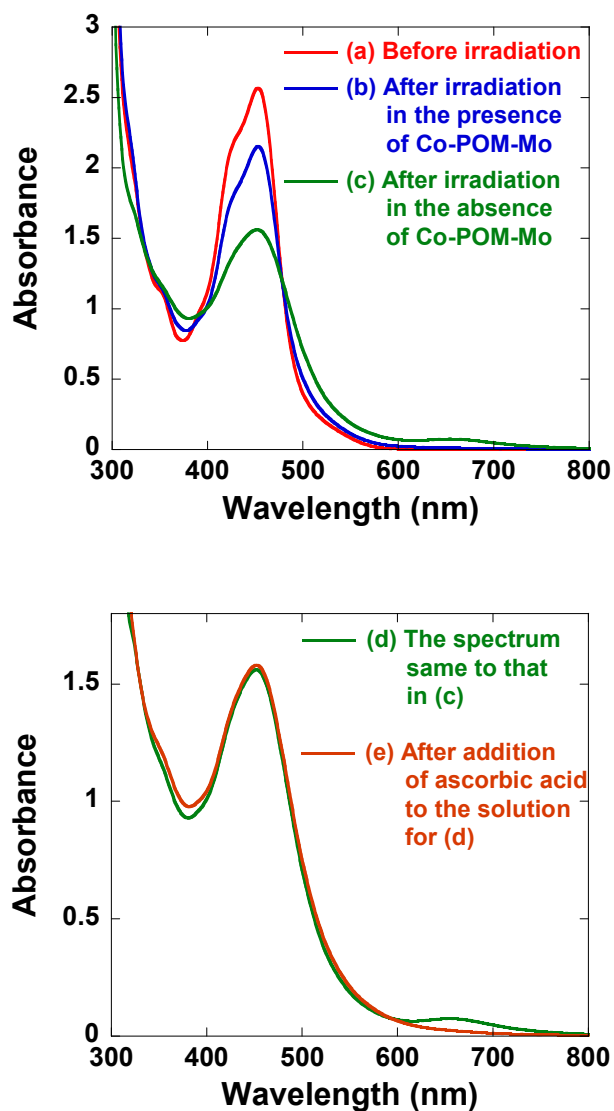
Fig. S5 The figure in the top shows the spectral changes during the photochemical O_2 production in Ar at 20 °C (irradiation with 300 W Xe). Spectrum (a) shows a UV-visible absorption spectrum of an aqueous borate buffer solution (0.1 M, pH = 8.0) containing $[Ru(bpy)_3](NO_3)_2·3H_2O$ (0.2 mM) and $Na_2S_2O_8$ (3.0 mM). Spectra (b) and (c) correspond to those recorded after 20-min irradiation with 300 W Xe in the presence and absence of **Co-POM-Mo** (20 μM), respectively. The figure in the bottom shows the spectrum same to that in (c) (spectrum (d)) and that observed after adding an excess of ascorbic acid to the solution used for the spectrum (d) (spectrum (e)), where the 675-nm band ascribable to the LMCT band of $Ru^{III}(bpy)_3^{3+}$ could be bleached but the recovery in the MLCT band is meaningless, confirming that the major cause of the decrease in absorbance at the MLCT band (455 nm) is due to the unrecoverable photodegradation of $Ru(bpy)_3^{2+}$.
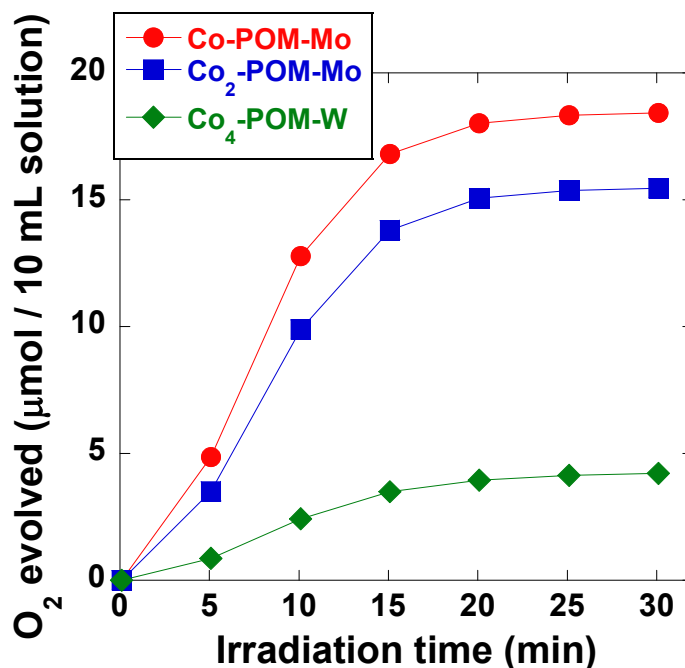
Fig. S6 Photochemical O_2 production from an aqueous borate buffer solution (0.1 M, pH = 8.0; 10 mL) containing $Na_2S_2O_8$ (5.0 mM) and $[Ru(bpy)_3](NO_3)_2 \cdot 3H_2O$ (0.4 mM) catalyzed by **Co-POM-Mo** (20 µM; ●), **Co₂-POM-Mo** (10 µM; ■), and **Co₄-POM-W** (5 µM; ♦) in Ar at 20 °C (irradiation with 300 W Xe). The initial slopes of O_2 evolution were determined as 1.28 µmol/min for **Co-POM-Mo** and 0.989 µmol/min for **Co₂-POM-Mo**. The photolysis experiments were carried out by using an interference filter, Asahi Spectra SV 490 and several neutral density filters to diminish the transmittance to 7.2%.
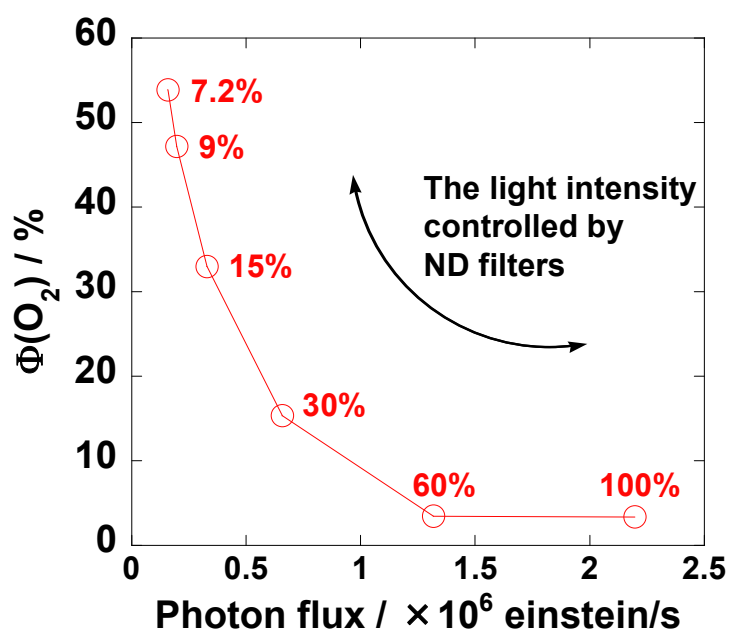
Fig. S7 Photochemical O_2 production from an aqueous borate buffer solution (0.1 M, pH = 8.0; 10 mL) containing $Na_2S_2O_8$ (5.0 mM) and $[Ru(bpy)_3](NO_3)_2 \cdot 3H_2O$ (0.4 mM) catalyzed by **Co-POM-Mo** (20 μM) in Ar at 20 °C (irradiation with 300 W Xe). The photolysis experiments were carried out as a function of the photon flux by using an interference filter, Asahi Spectra SV 490. The values shown in red show the transmittance controlled by use of several neutral density filters. The quantum yields for the photochemical O_2 evolution ($\Phi(O_2)$) are plotted as a function of the photon flux.
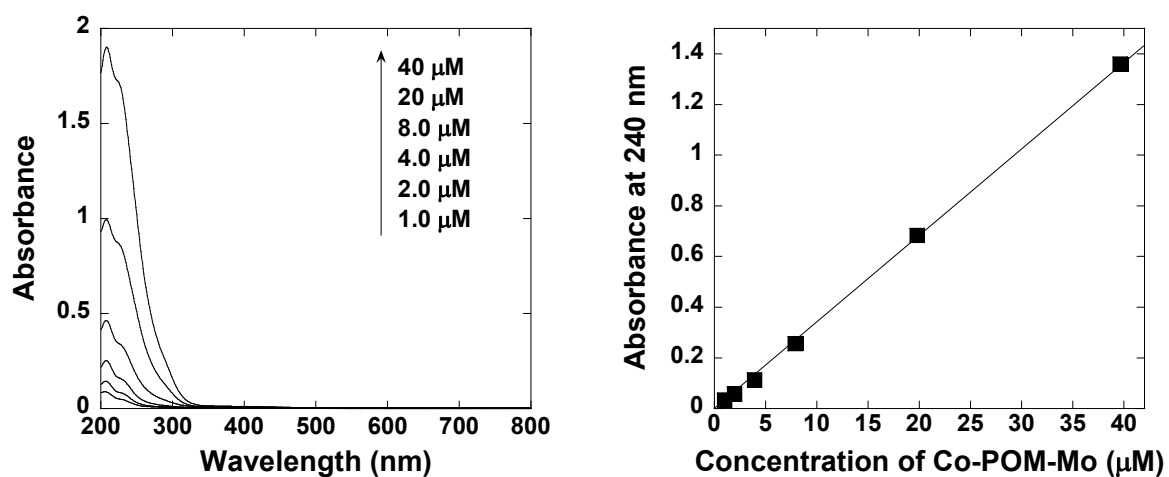
Fig. S8 (Left) UV-vis absorption spectra of **Co-POM-Mo** in aqueous solution at various concentrations under air at at 20 °C. (Right) The concentration dependence of absorbance at 240 nm in the concentration range of 1.0−40 μM, showing that the Beer's law is obeyed and **Co-POM-Mo** is not likely to form a dimer nor oligomer in aqueous media.
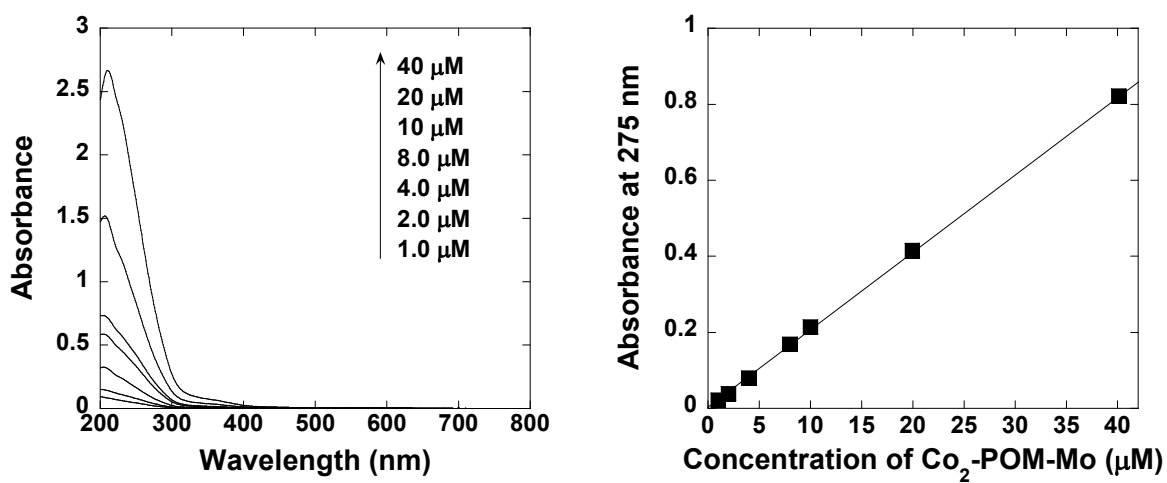
Fig. S9 (Left) UV-vis absorption spectra of **Co₂-POM-Mo** in aqueous solution at various concentrations under air at at 20 °C. (Right) The concentration dependence of absorbance at 275 nm in the concentration range of 1.0−40 μM, showing that the Beer's law is obeyed and **Co₂-POM-Mo** is not likely to form a dimer nor oligomer in aqueous media.
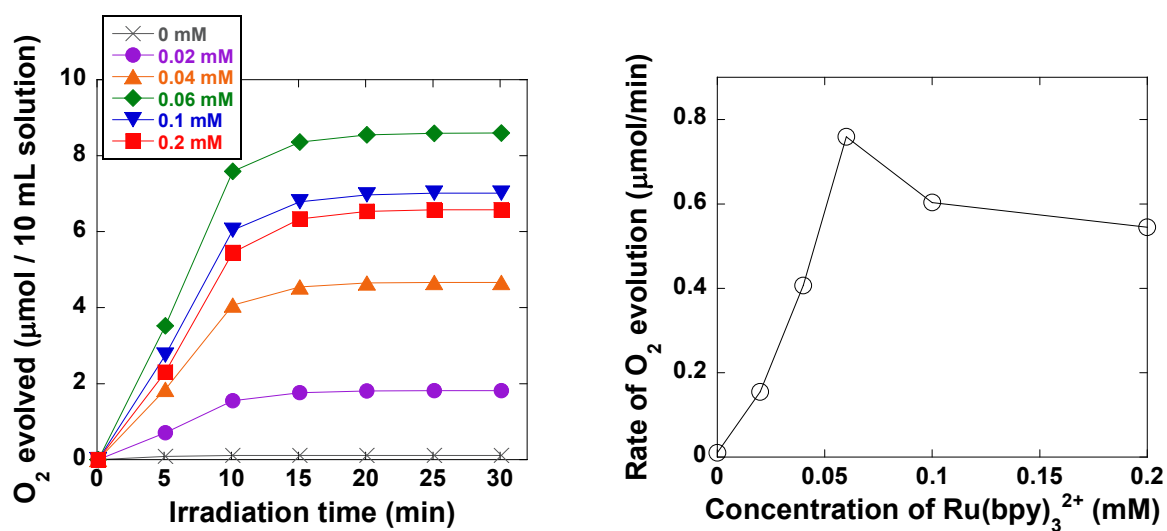
Fig. S10 Photochemical O_2 production from an aqueous borate buffer solution (0.1 M, pH = 8.0; 10 mL) containing $Na_2S_2O_8$ (3.0 mM) and **Co-POM-Mo** (20 μM) in the presence of $[Ru(bpy)_3](NO_3)_2 \cdot 3H_2O$ at various concentrations (0.0−0.2 mM) in Ar at 20 °C (irradiation with 300 W Xe). The initial slopes of O_2 formation curves are plotted as a function of the $[Ru(bpy)_3](NO_3)_2 \cdot 3H_2O$ concentration.
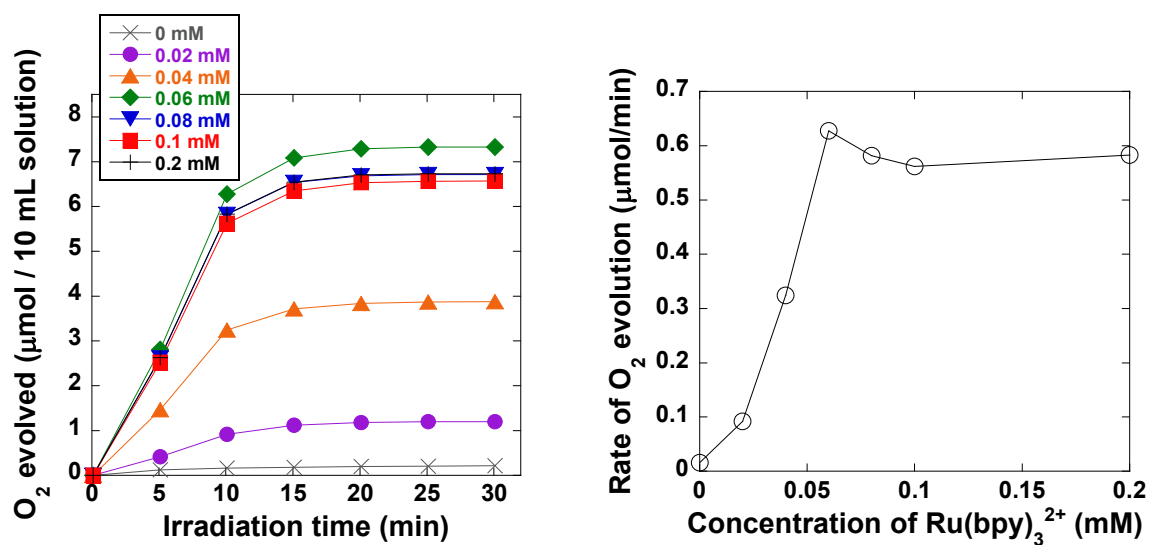
Fig. S11 Photochemical O_2 production from an aqueous borate buffer solution (0.1 M, pH = 8.0; 10 mL) containing $Na_2S_2O_8$ (3.0 mM) and **Co$_2$-POM-Mo** (10 μM) in the presence of $[Ru(bpy)_3](NO_3)_2 \cdot 3H_2O$ at various concentrations (0.0−0.2 mM) in Ar at 20 °C (irradiation with 300 W Xe). The initial slopes of O_2 formation curves are plotted as a function of the $[Ru(bpy)_3](NO_3)_2 \cdot 3H_2O$ concentration.
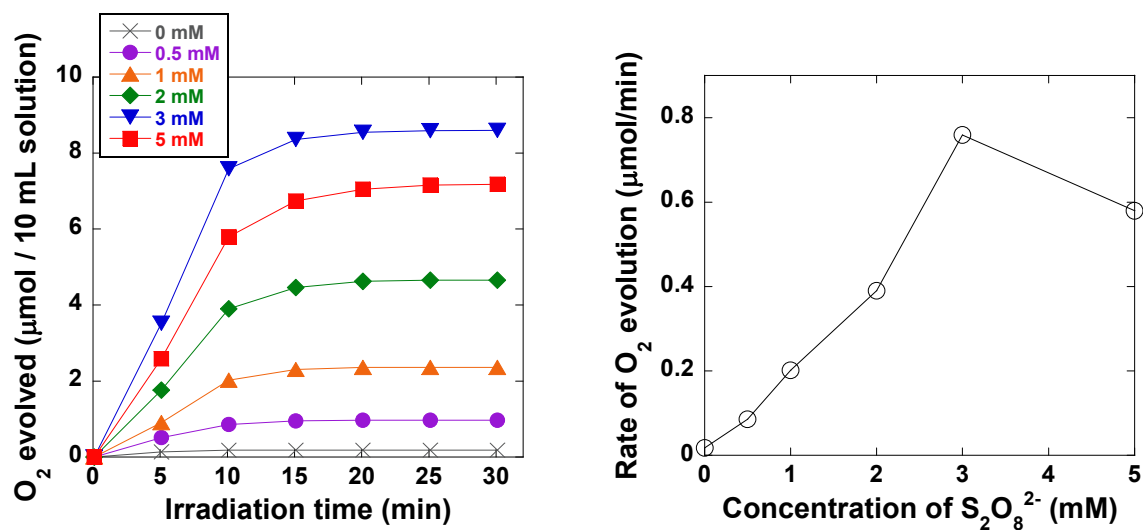
Fig. S12 Photochemical O_2 production from an aqueous borate buffer solution (0.1 M, pH = 8.0; 10 mL) containing $[Ru(bpy)_3](NO_3)_2 \cdot 3H_2O$ (0.06 mM) and **Co-POM-Mo** (20 μM) in the presence of $Na_2S_2O_8$ at various concentrations (0.0−5.0 mM) in Ar at 20 °C (irradiation with 300 W Xe). The initial slopes of O_2 formation curves are plotted as a function of the $Na_2S_2O_8$ concentration.
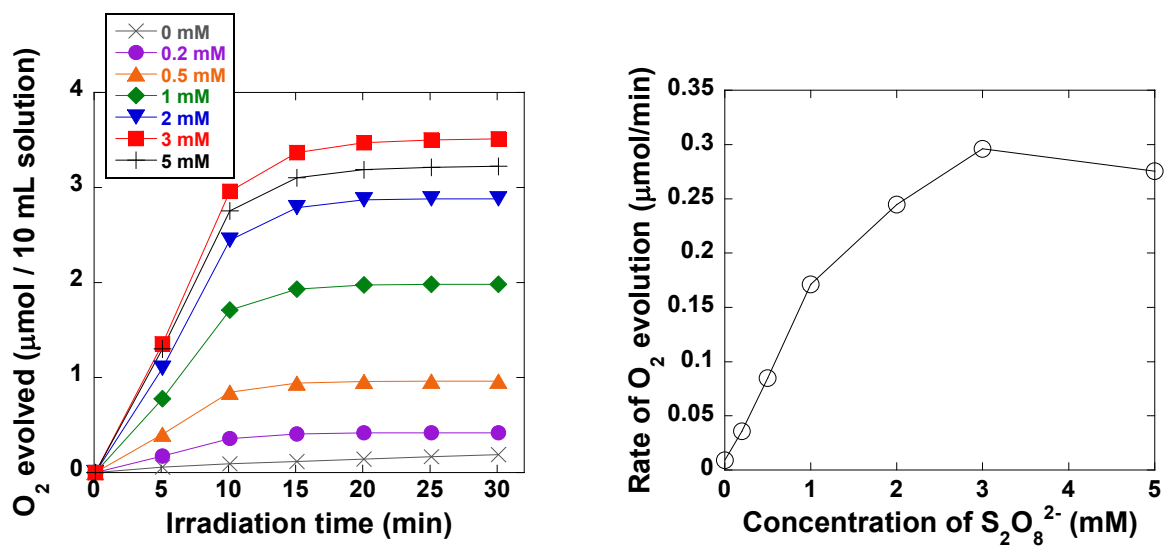
Fig. S13 Photochemical O_2 production from an aqueous borate buffer solution (0.1 M, pH = 8.0; 10 mL) containing $[Ru(bpy)_3](NO_3)_2 \cdot 3H_2O$ (0.04 mM) and **Co$_2$-POM-Mo** (20 μM) in the presence of $Na_2S_2O_8$ at various concentrations (0.0−5.0 mM) in Ar at 20 °C (irradiation with 300 W Xe). The initial slopes of O_2 formation curves are plotted as a function of the $Na_2S_2O_8$ concentration.
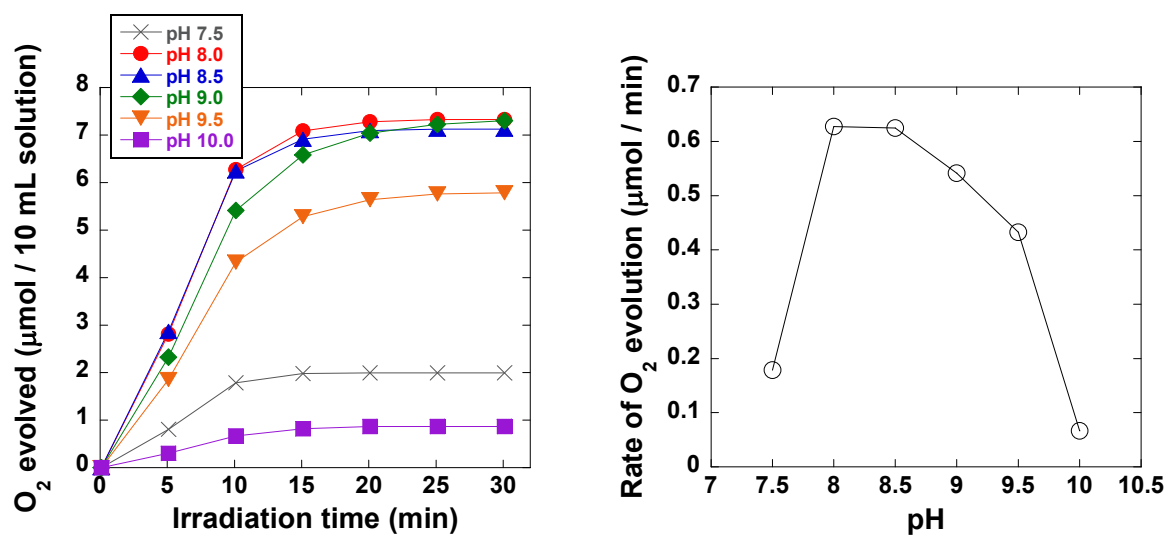
Fig. S14 Photochemical O_2 production from an aqueous borate buffer solution (0.1 M; 10 mL) containing $Na_2S_2O_8$ (3.0 mM) and $[Ru(bpy)_3](NO_3)_2 \cdot 3H_2O$ (0.06 mM) catalyzed by **Co_2-POM-Mo** (10 μM) at various pH conditions (7.5−10.0) in Ar at 20 °C (irradiation with 300 W Xe). The initial slopes of O_2 formation are plotted as a function of pH.
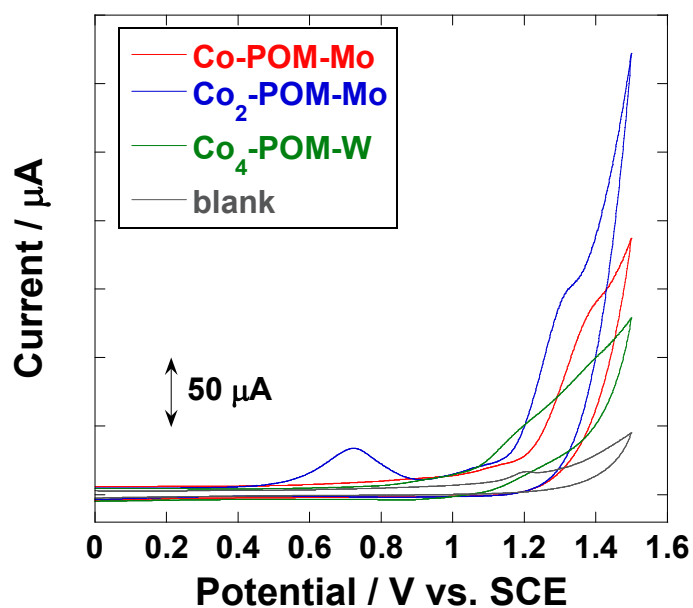
Fig. S15 Cyclic voltammograms of **Co-POM-Mo** (1 mM; red line), **Co$_2$-POM-Mo** (1 mM; blue line) and **Co$_4$-POM-W** (1 mM; green line) in an aqueous borate buffer solution (0.1 M, pH = 8.0) containing 0.1 M KNO$_3$ as a supporting electrolyte at a scan rate of 50 mV/s under Ar, where a glassy carbon, a platinum wire, and a saturated calomel electrodes were used as a working, counter, and reference electrodes, respectively.

Table S1 Photochemical O_2 production catalyzed by **Co$_n$-POM-Mo**.[a]

Catalyst (µM)	[Ru(bpy)$_3$]$^{2+}$ (mM)	S$_2$O$_8$$^{2-}$ (mM)	O$_2$[b] (µmol)	TON[c]	Chemical yield[d]	Quantum yield[e]
Co-POM-Mo (1.2)	0.06	3	1.14	97.7	0.0759	
Co-POM-Mo (1.8)	0.06	3	2.04	112	0.136	
Co-POM-Mo (3.6)	0.06	3	3.82	107	0.255	
Co-POM-Mo (9.2)	0.06	3	6.81	73.8	0.454	
Co-POM-Mo (20)	0.06	3	8.59	43.4	0.573	
Co-POM-Mo (40)	0.06	3	7.47	18.8	0.498	
Co-POM-Mo (0)	0.06	3	0.026	-	0.00174	
Co-POM-Mo (20)	0	3	0.11	0.56	0.00735	
Co-POM-Mo (20)	0.06	0	0.18	0.91	-	
Co$_2$-POM-Mo (0.99)	0.04	3	1.83	185	0.122	
Co$_2$-POM-Mo (2.0)	0.04	3	2.80	138	0.187	
Co$_2$-POM-Mo (5.1)	0.04	3	3.20	62.9	0.213	
Co$_2$-POM-Mo (9.8)	0.04	3	3.87	39.4	0.258	
Co$_2$-POM-Mo (20)	0.04	3	3.50	17.4	0.233	
Co$_2$-POM-Mo (10)	0	3	0.21	2.35	0.0156	
Co$_2$-POM-Mo (20)	0.04	0	0.19	0.92	-	
Co$_2$-POM-Mo (1.9)	0.06	3	2.95	154	0.197	
Co-POM-Mo (20)	0.4	5	18.4	93.4	0.737	0.539
Co$_2$-POM-Mo (10)	0.4	5	15.5	152	0.618	0.417
[Mo$_7$O$_{34}$]$^{6-}$ (10)	0.06	3	0.180	1.80	0.0120	
[PMo$_{12}$O$_{40}$]$^{3-}$ (10)	0.06	3	0.123	1.23	0.00822	

[a] O_2 production from an aqueous borate buffer solution (0.1 M, pH = 8; 10 mL) irradiated with 300 W Xe lamp (400−800 nm) at 20 ºC in Ar in the presence of additional components listed in this table. [b] The total amount of O_2 evolved from a 10 mL solution after 30 min of irradiation. [c] Based on the amount of O_2 evolved after 30 min of irradiation. [d] The yield of O_2 based on the persulfate consumed. [e] Based on the initial O_2 formation rate and photon flux. The photolysis experiments were carried out by using an interference filter, Asahi Spectra SV 490 and several neutral density filters to diminish the transmittance to 7.2%.

References

1   K. Sakai, Y. Kizaki, T. Tsubomura and K. Matsumoto, *J. Mol. Catal.*, 1993, **79**, 141.

2   C. G. Hatchard and C. A. Parker, *Proc. R. Soc. London, Ser. A.*, 1956, **235**, 518.